https://dx.doi.org/10.1016/j.oceaneng.2018.01.023

Identifying parameters of easily crushable sand and application to offshore pile driving

Yin-Fu JIN[1,2,3]; Zhen-Yu YIN[1,2,*]; Ze-Xiang WU[1,2,*]; Wan-Huan ZHOU[3]

Affiliation:

[1] Research Institute of Civil Engineering and Mechanics (GeM), UMR CNRS 6183, Ecole Centrale de Nantes, France

[2] Department of Geotechnical Engineering, College of Civil Engineering, Tongji University, Shanghai, China. Key Laboratory of Geotechnical and Underground Engineering of Ministry of Education, Tongji University, Shanghai 200092, P. R. China.

[3] Department of Civil and Environmental Engineering, Faculty of Science and Technology, University of Macau, Macau.

[*] Corresponding author, Dr Zhen-Yu YIN, Tel: +33 240371588 / Fax: +33 240372535; E-mail: zhenyu.yin@gmail.com

Abstract: The estimation of the bearing capacity of driven piles of offshore platform in easily crushable sand is a big issue due to the difficulty of parameter identification. The paper proposes an efficient optimization procedure for identifying parameters of easily crushable sand which is then applied to the pile driving simulation. The Nelder-Mead Simplex genetic algorithm (NMGA) is first proposed and a newly enhanced elasto-plastic breakage model is adopted. Then, the performance of NMGA is validated by identifying parameters from synthetic tests, and further verified by triaxial tests on limestone grains, based on which the necessary number of objective tests are also suggested. Finally, the proposed procedure is applied to identify parameters of carbonate marine sand, and the Coupled Eulerian Lagrangian based large deformation analysis combined with the breakage model is carried out for pile driving in the same sand. The role of grain breakage in bearing capacity of driven pile is also discussed. All comparisons demonstrate that the proposed NMGA with breakage model based parameter identification procedure is efficient and effective for easily crushable sand, and the established large deformation analysis of pile driving using the identified parameters is applicable in estimating the bearing capacity.

Key words: Sand, parameter identification; grain breakage; optimization; genetic algorithm; pile penetration

1. Introduction

Foundations of offshore platforms are in the majority of cases piled-based, which are the most common foundation system due to their lower cost and simplicity and mainly driven to a certain design depth using hammers (Randolph et al., 2005). The most common problems for driven piles are associated with insufficient capacity (as indicated by driving performance or dynamic monitoring) at the end of driving. The capacity of driven piles in sands was identified by Randolph et al. (1994) as being the "area of greatest uncertainty in foundation design".

During the process of pile driven, grain breakage commonly occurs when sand undergoes compression and shearing, especially for sand with low Mohr's hardness mineral (e.g. Gypsum, Calcite and Fluorite with Mohr's hardness less than 4) even under very low confining stress, which is defined as "easily crushable sand" in this paper. From a different viewpoint, Zhang et al. (2016) used fracture mechanics and energy arguments to demonstrate the equivalence between measures of crushability based on yielding stress and measures of crushability based on energy input and dissipation. In either case, it is the fracture properties of the grain-forming mineral that controls the macroscopic crushability. More recently, it was shown that such link between macroscopic crushability and grain-scale fracture can be used to develop constitutive models at continuum scale (Zhang and Buscarnera, 2017).

The impact of grain breakage on the mechanical behavior of granular materials has been highlighted in the past decades (Coop, 1990; Coop et al., 2004; Lo and RoY, 1973; Miao and Airey, 2013). In order to describe the effect of grain breakage, numerous constitutive methods considering the grain breakage have been developed (Cecconi et al., 2002; Chen et al., 2015; Daouadji et al., 2001; Einav, 2007; Hu et al., 2011; Kong et al., 2017; Liu and Gao, 2016; Russell and Khalili, 2004; Xiao and Liu, 2016; Yao et al., 2008a; Yin et al., 2016). Especially in advanced breakage models incorporating the critical state concept, additional parameters are introduced which are difficult to be determined by conventional laboratory or field tests. Especially in advanced breakage models incorporating the critical state concept, additional parameters are introduced which are difficult to be determined by conventional laboratory or field tests. For instance, in critical state based breakage models, the critical state line kinematically moves with the amount of grain crushed. Thus, the

critical state related parameters, the hardening parameters and the dilatancy parameters become much more difficult to be calibrated in breakage model than in conventional critical state based models, such as the critical state line related parameters (e.g., υ_f and λ_f) in the model of Russell and Khalili (2004); the critical state parameters (e_{ref0} and λ) in the model of Hu et al. (2011); the critical state parameters ($e_{\Gamma i}$, ϕ_{cr}, and λ), the dilatancy parameters (k_d and A) and the hardening parameters (ξ_{L0}, ξ_L, ξ_U, and γ) in the model of Chen et al. (2015) ; the critical state related parameters (λ, e_{B0}, k_e, and χ_B) and two dilatancy constants (d_0 and k_d) in the model of Xiao and Liu (2016). This difficulty is much more pronounced for very easily crushable sand, and poses a challenge in terms of engineering practice. As a consequence, the breakage models were seldom used in the engineering practice. To improve the determination of parameters, more laboratory tests are becoming necessary, which results in a relatively high experimental cost. Therefore, an efficient approach to identify model parameters by a cost-saving way is useful and will be attractive for engineering practice.

Recently, the optimization method based on genetic algorithm (GA) has been applied successfully in the geotechnical engineering since its application can reduce the cost of laboratory testing or in situ monitoring. For example, the parameter identifications of various constitutive models for different soils have been carried out using optimizations with GA (Jin et al., 2017a; Jin et al., 2017b; Jin et al., 2016b; Jin et al., 2017c; Levasseur et al., 2008; Pal et al., 1996; Papon et al., 2012; Rokonuzzaman and Sakai, 2010; Samarajiva et al., 2005; Ye et al., 2016; Yin et al., 2017a; Yin et al., 2017b). Along this way, it will be attractive if this powerful tool can be applied to identify parameters of breakage models for easily crushable sand.

Therefore, this study aims to propose an efficient optimization procedure for identifying parameters of easily crushable sand based on conventional laboratory tests which is then applied to the pile driving simulation. For this purpose, a recently enhanced elasto-plastic breakage model is adopted for simulations. A novel Nelder-Mead Simplex enhanced genetic algorithm (NMGA) is developed to minimize the error function during the optimization process. Then, the parameter identification using three synthetic drained triaxial tests generated by the adopted model as objective tests is conducted to evaluate the performance of NMGA. After that, the model parameters for limestone grains are identified using the proposed optimization procedure with discussions on the

necessary number of objective tests. Finally, the proposed procedure is applied to identify parameters of Dog's bay sand using four triaxial tests and validated by three other triaxial tests. The Coupled Eulerian Lagrangian based large deformation finite element analysis combined with the breakage model is carried out for pile driving in the same sand for which the finite element implementation of the model is also presented. Furthermore, the role of grain breakage in bearing capacity of driven pile is numerically discussed.

2. Adopted elasto-plastic grain breakage model

A novel constitutive model accounting for the effect of grain breakage developed by Yin et al. (2016a) was adopted to simulate the experiment in the optimization process. The total strain rate is conventionally composed of the elastic and plastic strain rates:

$$\dot{\varepsilon}_{ij} = \dot{\varepsilon}_{ij}^{e} + \dot{\varepsilon}_{ij}^{p} \tag{1}$$

The elastic behavior is assumed to be isotropic with the bulk modulus K adopting the same form of the shear modulus proposed by Richart et al. (1970),

$$\dot{\varepsilon}_{ij}^{e} = \frac{1+\upsilon}{3K\left(1-2\upsilon\right)}\sigma'_{ij} - \frac{\upsilon}{3K\left(1-2\upsilon\right)}\sigma'_{kk}\delta_{ij} \tag{2}$$

$$K = K_0 \cdot p_{at}\frac{\left(2.97-e\right)^2}{\left(1+e\right)}\left(\frac{p'}{p_{at}}\right)^{\zeta} \tag{3}$$

where K_0 and ζ are elastic parameters; υ is Poisson's ratio; p' is the mean effective stress; p_{at} is the atmospheric pressure used as reference pressure (p_{at} = 101.3 kPa); δ_{ij} is the Kronecker delta.

The adopted model contains two yield surfaces: one for shear sliding (f_1) and one for compression (f_2). The plastic strain increment can be expressed as follows,

$$\dot{\varepsilon}_{ij}^{p} = \dot{\varepsilon}_{ij}^{p1} + \dot{\varepsilon}_{ij}^{p2} = \mathrm{d}\lambda_1\frac{\partial g_1}{\partial \sigma'_{ij}} + \mathrm{d}\lambda_2\frac{\partial g_2}{\partial \sigma'_{ij}} \tag{4}$$

where the scripts 1 and 2 represent the shear sliding and compression components, respectively. For one component with $f < 0$, the corresponding $\mathrm{d}\lambda$ is equal to zero.

The shear sliding yield function, noted f_1 has the following expression,

$$f_1 = \frac{q}{p'} - \frac{M_p \varepsilon_d^p}{\left(M_p p'\right)/\left(G_p G\right) + \varepsilon_d^p} = 0 \tag{5}$$

where the deviatoric plastic strain ε_d^p is the hardening variable, q is the deviatoric stress ($q=\sqrt{3J_2} = \sqrt{3/2}\sqrt{s_{ij}s_{ji}}$ with $s_{ij} = \sigma_{ij} - p'\delta_{ij}$); p' is the mean effective stress; G_p is the relative plastic stiffness controlling the hardening rate; G is shear modulus which can be calculated using the K and υ; $M_p = 6\sin(\phi_p)/(3-\sin(\phi_p))$ is the stress ratio corresponding to the peak strength and determined by the peak friction angle ϕ_p.

The plastic potential function is given by,

$$\frac{\partial g_1}{\partial \sigma'_{ij}} = \frac{\partial g_1}{\partial p'}\frac{\partial p'}{\partial \sigma'_{ij}} + \frac{\partial g_1}{\partial s_{ij}}\frac{\partial s_{ij}}{\partial \sigma'_{ij}} \quad \text{with} \quad \frac{\partial g_1}{\partial p'} = A_d\left(M_{pt} - \frac{q}{p'}\right);\ \frac{\partial g_1}{\partial s_{ij}} = \{1 \quad 1 \quad 1 \quad 1 \quad 1 \quad 1\} \tag{6}$$

where g_1 is different from f_1; therefore, the model is non-associated. A_d is the stress-dilatancy parameter; $M_{pt} = 6\sin(\phi_{pt})/(3-\sin(\phi_{pt}))$ where ϕ_{pt} phase transformation friction angle. The double indices ij is simplified to be $1 \hat{=} 11,\ 2 \hat{=} 22,\ 3 \hat{=} 33,\ 4 \hat{=} 12,\ 5 \hat{=} 23,\ 6 \hat{=} 31$ according to the Voigt rule since stress or strain tensors are symmetric.

The peak friction angle ϕ_p and the phase transformation friction angle ϕ_{pt} are associated with the critical friction angle, ϕ_μ and the critical void ratio, e_c is as follows:

$$\tan\phi_p = \left(\frac{e_c}{e}\right)^{\beta}\tan\phi_u; \quad \tan\phi_{pt} = \left(\frac{e_c}{e}\right)^{-\beta}\tan\phi_\mu \tag{7}$$

$$e_c = e_{ref} - \lambda\ln\left(\frac{p'}{p_{ref}}\right) \tag{8}$$

where β is a material constant, commonly equal to 1 according to Yin et al. (2016a). λ is the slope of the critical state line in the e-lnp' plane; the two parameters (e_{ref}, p_{ref}) correspond to a reference point on the critical state line (CSL). The lode angle dependent strength and stress-dilatancy were introduced as described in Yin et al. (2013), which can also be incorporated by using the transformed stress method by (Yao et al., 2009; Yao et al., 2004a; Yao et al., 2004b; Yao et al., 2008b).

In order to describe the compression behavior of crushable sand, a second yield surface was added,

$$f_2 = \frac{1}{2}\left(\frac{q}{p'M_p}\right)^3 p' + p' - p_m \quad \text{for } \frac{q}{p'} \le M_p \tag{9}$$

where p_m is the hardening variable controlling the size of the yield surface. An associated flow rule is adopted herein. This yield surface expands with the plastic volumetric strain, as in the modified Cam Clay model

$$p_m = p_{m0}\exp\left(\frac{1+e_0}{\lambda-\kappa}\varepsilon_v^p\right) \tag{10}$$

where $\kappa = (1+e_0)p'/K$ is used with K by Eq.(3); λ takes the same value as that of the CSL.

The effects of grain breakage on the mechanical behavior can be expressed in two aspects:

(1) Influence of grain breakage on the critical state line. The evolution of the critical state line due to grain breakage is described as following expression,

$$p_{ref} = p_{ref\,0}\exp\left(-bB_r^*\right) \tag{11}$$

where parameter b controls the rate of the CSL shifting due to grain breakage; B_r^* is the modified breakage index proposed by Einav (2007), which can be considered as a function of the plastic work during loading,

$$B_r^* = \frac{w_p}{a + w_p} \tag{12}$$

where a is a material constant controlling the evolution of the breakage amount.

Grain breakage was classified into three modes according to Guyon and Troadec (1994): (1) fracture which means a grain breaks into smaller grains of similar sizes, (2) attrition which means a grain breaks into one grain of a slightly smaller size and several much smaller ones, (3) abrasion which means the result is that the grain size distribution remains almost constant but with a production of fine particles. These three modes also associate with the applied stress level: from low pressure to high pressure, the grain breakage from the model (3) to mode (1) dominates. The Eq.(12) follows this phenomenon. Note that there exists a threshold plastic work or stress level from a physical standpoint for which one more parameter needs to be introduced. In fact this threshold value is questionable in terms of parameter calibration since the grain breakage of mode (3) cannot be

clearly measured. Fortunately, the Eq.(12) can capture very slight amount of grain breakage corresponding to mode (3) mainly due to inter-particle shear sliding at low stress level.

(2) Influence of grain breakage on compression behavior. The evolution of p_m due to grain breakage is added in Eq.(13) as follow,

$$p_m = p_{m0} \exp\left(\frac{1+e_0}{\lambda-\kappa}\varepsilon_v^p\right)\exp\left(-bB_r^*\right) \tag{13}$$

Note that the same constant b is used in Eq.(13) and Eq.(11) implying the same amount of shifting for isotropic compression line and critical state line, which was previously validated by Yin et al. (2016). Furthermore, the Eq.(13) also assumed that the size of yield surface is controlled by two factors simultaneously: the volumetric plastic strain and the modified breakage index.

Overall, the parameters of the adopted breakage model can be divided into four groups: (1) elastic parameters (K_0, n, υ); (2) critical-state related parameters (e_{ref}, λ, ϕ_u); (3) plastic parameters (G_p, A_d); and (4) grain breakage related parameters (p_{m0}, a, b).

3. Identification methodology

In general, the mathematical procedure of optimization consists of two parts: (a) the formulation of an error function measuring the difference between the numerical and experimental results, and (b) the selection of an optimization strategy to enable the search for the minimum of this error function.

3.1. Error function

To carry out a parameter identification using optimization method, the user must define a function that can evaluate the error between the experimental and numerical results, and then minimize this function. For the optimization to be successful, it is necessary to evaluate the accuracy of the material parameter sets' predictions as accounted for in terms of a fitness function. The material parameter sets with higher fitness should survive to produce new parameters sets. Therefore, it is necessary to devise an error function so that the parameter sets with better predictions result in higher fitness values.

To make the error independent of the type of test and the number of measurement points, an advanced error function can be adopted (Levasseur et al., 2008). The average difference between the measured and the simulated results is expressed in the normalized form of the least square method,

$$\text{Error}(x)=\sqrt{\frac{1}{N}\sum_{i=1}^{N}\left(\frac{U_{\exp}^{i}-U_{num}^{i}}{U_{\exp}^{i}}\right)^{2}}\times 100 \tag{14}$$

where x is an n-sized vector of unknown model input parameters; N is the number of observation points. U_i^{obs} is the value corresponding to the ith point of observed data; U_i^{num} is the value corresponding to the ith point of simulated data.

The scale effects on the fitness between the experimental and the simulated results can be eliminated by this normalized formula. Additionally, the objective error calculated by this function is a dimensionless variable, thus, any difference in error can be avoided for different objectives with different variables. Due to the stability of Eq.(14), many researchers have adopted it as the error function to conduct the optimizations (Jin et al., 2017a; Jin et al., 2016b; Jin et al., 2017c; Yin et al., 2017a; Yin et al., 2017b).

3.2. Enhancement of RCGA algorithm

After formulating the error function, the selection of the search strategy is the key step of whether the optimized solution can be found or not. The solution to an optimization problem is a vector x_0 which satisfies the global minimum condition for any $x_l \ll x \ll x_u$,

$$F(x_0)\le F(x) \tag{15}$$

For obtaining a more accurate solution, a highly efficient optimization method with the ability to search for a global minimum should be adopted. Since the GA is widely used in the geotechnical field as stated in the introduction, the adopted real-coded GA (RCGA) algorithm has a similar structure to those developed by Jin et al. (2016c) and Yin et al. (2017b) To further accelerate the convergence speed and enhance the search ability, the adopted RCGA was enhanced by implementing a local search named “Nelder-Mead Simplex (NMS)” with excellent convergence speed. The proposed algorithm was named as “NMGA” for simplicity in the following sections.

Although the hybrid of Nelder-Mead optimization scheme and GA with its efficiency has been well recognized during past decades (Chelouah and Siarry, 2003; Durand and Alliot, 1999), on the premise of keeping the intrinsic advantage of hybrid between GA and Simplex, adopting newly developed optimization schemes is necessary and useful for solving complex geotechnical problems with more parameters. In this study, the NMGA is different from previous works (Chelouah and Siarry, 2003; Durand and Alliot, 1999) due to (1) the adoption of the newly developed RCGA with outstanding performance in identifying soil parameters and (2) a newly developed NMS operator for high dimensional problems. Fig. 1 shows the flow chart which presents the simplest way of the enhancement. First, *N* initial individuals were generated by SOBOL, which is a uniform sampling method proposed by Sobol (1967) and the generation number was set to zero. Then, all the individuals were sorted based on their fitness values, and the best n+1 (n is the number of variables) individuals were selected to perform the NMS. For the NMS, a Nelder-Mead method with adaptive parameters for high dimensional problems suggested by Gao and Han (2012) was adopted, and a brief procedure of this method is presented in Appendix I. Based on the result of the NMS, the best individual was updated. Then, this best individual was recombined with the n-1 remaining individuals to perform the GA global search. More details about the adopted RCGA can be found in Jin et al. (2016d). In order to avoid a rapid loss of diversity, an elitism strategy was adopted in the RCGA. In the replacement process, 10% of individuals with the highest fitness were selected from the parents and children to survive to the next generation. The remainders were chosen by tournament selection from the mating pool composed of parents and children other than the 10% individuals. The iteration stopped when the convergence criterion or the maximum generation number was reached.

For the NMS, the tolerance for convergence was set to 10^{-4}, as recommended by Gao and Han (2012). For the adopted RCGA, the recommended settings can be found in Jin et al. (2016d).

During the optimization process, the NMS could accelerate the convergence speed, but could easily get trapped in the local minimum. On the other hand, the RCGA process can overcome the local minimum problem, however, the convergence speed is always slow and the approach is not applicable for the engineering applications (Jin et al., 2017b; Jin et al., 2016b; Yin et al., 2017b).

Therefore, this hybrid strategy owns the advantages of both processes and results in better optimization performance.

3.3. Proposed identification procedure

In general, deformation and strength are two important indicators of the mechanical behavior of granular materials. Additionally, the grain size distribution (GSD) is strongly associated with the grain breakage effect during the loading process and hence influence the mechanical behaviors (Liu et al., 2014), especially for the crushable materials. Therefore, the GSD is another indicator for measuring the degree of gain breakage. For a laboratory triaxial test, the isotropic or anisotropic compression test is normally first conducted, followed by the shearing test. During the whole testing process, the measurements indicating the compression behavior, shearing behavior and grain breakage behavior are recorded. Some model parameters can be directly determined based on the measurements, e.g., the initial void ratio, Young's modulus (Jin et al., 2016a; Jin et al., 2016c). While some variables cannot be directly measured, e.g., the parameters related to grain breakage (Chen et al., 2015; Hu et al., 2011). Therefore, the parameter identification using optimization method is proposed. In this study, a mono-objective framework with 4 different criteria is considered:

$$\min\left[\mathrm{Error}(x)\right] = \min\left\{\mathrm{mean}\left[\mathrm{Error}_{\mathrm{com}}(e), \mathrm{Error}_{\mathrm{tri}}(q), \mathrm{Error}_{\mathrm{tri}}(e), \mathrm{Error}_{\mathrm{com+tri}}(\mathrm{GSD})\right]\right\} \quad (16)$$

where $\mathrm{Error}_{\mathrm{com}}$ (e) is the error of void ratio e between simulations and objectives for isotropic compression or anisotropic compression stage; $\mathrm{Error}_{\mathrm{tri}}$ (q) is the error in deviatoric stress q between simulations and objectives for the triaxial shearing stage; $\mathrm{Error}_{\mathrm{tri}}$ (e) is the error in void ratio e between simulation and objectives for triaxial shearing stage, and $\mathrm{Error}_{\mathrm{com+tri}}$ (GSD) is the error in GSD curve between simulations and objectives for both compression and triaxial shearing stage. All the errors mentioned above were calculated according to the Eq.(14).

Fig. 2 shows the identification procedure which aims to find values for the model parameters and provide the best attainable fit between model predictions and corresponding observations. In this study, the procedure is based on two different codes: the code for the integration of the constitutive model to simulate the objective tests and the code for the optimization process to find the minimum value of error function. For each optimization process, each individual in the initial population was generated using the SOBOL method (Sobol, 1967).

3.4. Performance of NMGA on identifying model parameters

For evaluating the performance of the proposed NMGA, a set of synthetic tests including three drained triaxial tests (e_0 = 0.8 with p_0 = 100, 200 and 400 kPa) and one isotropic compression test (e_0 = 0.8) was generated by the adopted breakage model (Yin et al., 2016) as the objectives in the optimization. In order to simulate the breakage behavior of easily crushable materials, a set of typical parameters: the elastic parameters (K_0=70, n=0.66, υ=0.25), the critical-state related parameters (e_{ref} =1.0, λ=0.05, ϕ=35), the plastic parameters (G_p=5, A_d=1), and the grain breakage related parameters (p_{m0}=500 kPa, a=150 kPa, b = 10) was adopted to generate the synthetic tests, and the simulated results are shown in Fig. 3. Totally 10 model parameters were optimized by using the proposed optimization procedure, as shown in Eq.(17).

$$\min f_e(x) = \min f_e\left(K_0,\ n,\ e_{ref},\ \lambda,\ \phi,\ G_p,\ A_d,\ p_{m0},\ a,\ b\right) \tag{17}$$

where f_e is the error function of the model parameters; x is the model parameters.

The initial population size was set to 100 and the maximum number of generations was set to 300. The interval of each parameter is given in Table 1, which covers a big range in terms of preset parameters. For comparison and verifying the performance of the proposed NMGA, the original RCGA without Nelder-Mead Simplex in Jin et al. (2016d) and another outstanding algorithm MOGA-II used by Papon et al. (2012) were selected to conduct the same optimization. Optimal parameters obtained by NMGA, RCGA and MOGA-II from synthetic data are summarized in Table 2. It can be seen that the preset parameters can be entirely detected within 300 generations by the proposed NMGA. However, the performance of RCGA and MOGA-II is worse satisfied comparing to that of the NMGA. Fig. 4 shows the evolution of minimum objective error in each generation with the increasing number of generations. It can be seen that the proposed NMGA has the faster convergence speed than the MOGA-II. Therefore, all the comparisons demonstrate that the proposed NMGA has an excellent performance on identifying model parameters for easily crushable sands.

4. Verification by limestone grains

4.1. Brief introduction of laboratory tests on limestone grains

In order to evaluate the effectiveness and efficiency of proposed optimization procedure, a series of conventional drained triaxial tests on limestone grains (a easily crushable sand, the Mohr's hardness equals to 3.5) by Lo and Roy (1973) was selected as objective tests. Some main physical properties of this limestone grains are as follows: specific gravity G_s=2.71, initial void ratio e_0=0.81, maximum void ratio e_{max}=1.05 and minimum void ratio e_{min}=0.65, mean particle size d_{50}=0.215 mm, uniformity coefficient C_u=2.85. For simplicity, all the tests with different confining pressures were marked by the sequence number. The sequence number and the information for the corresponding test are summarized in Table 3. Before conducting the triaxial shear test, each sample was compressed from the initial void ratio 0.81 to the corresponding confining pressure. After shearing, the change of grain size distribution for each sample was measured.

4.2. Optimization results and discussion

Following the proposed procedure, the model parameters for limestone grains were identified by the proposed NMGA. In addition, the RCGA and the MOGA-II were also adopted to conduct the same identification procedure for comparisons. For both adopted algorithms, the initial individuals and the maximum number of generations were set to 100. Other settings of RCGA recommended by Jin et al. (2016d) and MOGA-II recommended by Papon et al. (2012) were kept in this case. To highlight the performance of the proposed procedure in identifying breakage related parameters, the parameters related to compression behavior (K_0 = 24, n = 0.5 and p_{m0} = 1000 kPa) which can be directly measured from isotropic compression curve were not put into the optimization procedure. The Poisson's ratio υ is assumed to be 0.25 which is a typical value for sand. Furthermore, the remaining parameters (e_{ref}, λ, ϕ, G_p, A_d, a, b) can also be determined in a direct way according to Yin et al. (2016a) for sand that has a high yielding stress. However, for easily crushable sand, the direct way to determine these parameters (e_{ref}, λ, ϕ, G_p, A_d, a, b) based on laboratory tests is difficult due to the grain breakage occurring even in a very low stress level. Therefore, apart from the parameters related to compression behavior (K_0 = 24, n = 0.5 and p_{m0} = 1000 kPa), the remaining parameters (e_{ref}, λ, ϕ, G_p, A_d, a, b) were optimized using the proposed procedure. First, for obtaining a set of most

accurate parameters, all the experimental data (in total nine tests) was used as the objective in the optimization process. The objective error is defined as the average of $\mathrm{Error}_{\mathrm{com}}(e)$, $\mathrm{Error}_{\mathrm{tri}}(q)$, $\mathrm{Error}_{\mathrm{tri}}(e)$, and $\mathrm{Error}_{\mathrm{com+tri}}(\mathrm{GSD})$. The interval of each parameter is also given in Table 1.

Table 4 shows the comparison of optimal parameters and the corresponding objective error obtained by NMGA, RCGA and MOGA-II. It can be seen that the NMGA gives a set of optimal parameters with smallest objective error among them. Using the optimal parameters, the objective tests were simulated using the adopted breakage model. Fig. 5 shows the comparisons of "q-ε_a"(deviatoric stress versus axial strain), isotropic compression curve and GSD curves between simulated and experimental results. A good agreement between the simulations and observations indicates that the optimal parameters are reasonable and reliable, which also indicates that NMGA performs well in identifying breakage model parameters for easily crushable sand.

The convergence rates of NMGA, RCGA and MOGA-II are shown in Fig. 6. It can be seen that the convergence speed of NMGA is much faster than that of RCGA and MOGA-II, which indicates a higher efficiency of NMGA in the parameter identification. This should be attractive for engineering application.

Furthermore, for investigating the influence of the weight of GSD in the error function on optimized parameters, a scheme for evaluating the influence of the weight of GSD is presented in Table 5 based on the error function in Eq.(18).

$$\min\left[\mathrm{Error}(x)\right]=\min\left\{\left[\mathrm{mean}\left(A\left(\mathrm{Error}_{\mathrm{com}}(e),\mathrm{Error}_{\mathrm{tri}}(q),\mathrm{Error}_{\mathrm{tri}}(e)\right),(1-A)\mathrm{Error}_{\mathrm{com+tri}}(\mathrm{GSD})\right)\right]\right\} \tag{18}$$

where the A is weight factor varying between 0 and 1.

Following the same optimization procedure, the optimal parameters and objective errors corresponding to different weights of GSD are finally summarized in Table 5. It can be seen that the weight of GSD ranging from 0.3~0.7 gives a good performance in identifying the parameters of the adopted breakage model. Therefore, for obtaining an equal contribution of each term in the error function to the optimal parameters, the weight of GSD is set to 0.5. The following optimizations are then conducted based on the error function in Eq.(18) with a value of 0.5 for the weight of GSD.

4.3. Estimation of minimum number of tests for identifying parameters

Traditionally, three triaxial tests are needed for determining mechanical parameters of soils according to standard criterion of laboratory test. However, for determining parameters of critical-state-based models, more laboratory tests including isotropic compression and shearing stages are appreciated (Jin et al., 2016c). For easily crushable sand, it is questionable that how many tests are needed to determine the model parameters associated with grain breakage. It is clear that the process of parameter identification based on large number of tests is time-consuming and cost-consuming, which may not be preferred by the engineers. In order to reduce the test cost in parameter identification, the minimum number of tests involved in the objective to obtain a set of accurate parameters needs to be estimated.

Since the amount of grain breakage significantly associates with the applied stress level, two necessary tests, i.e. one test performed under a lower confining stress and one test performed under a higher confining stress, should be involved in the objective. Due to this, the tests ① and⑧ (see Table 3) were first selected as a basic component in all combinations (one combination is one objective for optimization), considering that the stress level of the test ⑧ is high enough. Then, combinations with three tests, or four tests, or five tests were constructed by adding one, or two, or three additional tests from database of tests ② to ⑦, based on which a total of 41 combinations were formed as seen in Table 6. All combinations were successively used for optimization to identify model parameters.

The examined combinations with the test number, the obtained optimal parameters, the objective error and the total average error are summarized in Table 6. Based on the total number of tests in the objective, all the combinations were divided into four groups and marked as “3 tests”, “4 tests”, “5 tests” and “8 tests”. Fig. 7 shows the minimum error and the average error in each group. It can be seen that both the average error and the minimum error generally decrease with the increasing number of tests in the objective. For some scatter points with big errors (as combinations 1, 2, 3, and 12), a possible reason is the inaccuracy of critical-state related parameters caused by the unreasonable selection of objective tests (Jin et al., 2016c). It can be seen that the minimum error and average error of the group containing four tests with more possible high stress tests or five tests is close to that obtained from 8 tests. In terms of the obtained optimal parameters, the average value of

each optimal parameter for each group has been calculated and is summarized in Table 7. It can be found that with increasing the quantity of tests in the objective, the obtained optimal parameters gradually approach to the most accurate set of parameters from all eight tests. The difference of the obtained optimal parameters, the objective error, and the total average error between the group with five tests and the group with all eight tests is very small, which can be ignored in the engineering practice. Therefore, it can be concluded that a total of four tests including two basic tests and two additional high stress tests, or a total of five tests including two basic tests and three additional tests are sufficient for the parameter identification.

5. Application to pile driving in carbonate sand

The pile driven in sand, especially in easily crushable sand, involves great amount of grain breakage. Thus, the numerical analysis of this kind of problem needs to consider the grain breakage effect in the mechanical behavior of sand. To date, various numerical studies on pile penetration in sand considering the grain breakage have been conducted (Zhang et al., 2013; Zhang et al., 2014). However, apart from grain breakage, nonlinear elasticity, dilatancy, and contraction with the soil density effect were not properly considered in those works, and the parameters were not fully calibrated against a series of laboratory tests on the same sand before the simulation. Accordingly, a case of pile driving in carbonate sand was selected as an illustrative example to highlight the proposed procedure in identifying parameters while the adopted model in simulating pile driven.

To exhibit the predictive ability of the adopted breakage model with validating the optimized parameters, a series of centrifuge tests by Klotz and Coop (2001), which is more realistic than the case of Zhang et al. (2013) in terms of field condition, were selected. These tests were conducted directly for the practical use on investigating the bearing capacity of offshore driven pile in very easily crushable sand. Furthermore, the choice of centrifuge tests using Dog’s Bay sand is also because that more laboratory tests on this sand with measurements of GSD before and after testing were provided than the case of Zhang et al. (2013).

This section presents the application of the proposed identification procedure to identify parameters of Dog's bay sand which was finally applied to the large deformation analysis of the pile driving in the same sand.

5.1. Parameter identification of Dog's bay sand

Four drained constant p' triaxial tests with different initial confining pressures by Bandini and Coop (2011) and one isotropic compression tests by Coop (1990) performed on Dog's bay sand were selected as the objective in the optimization. Due to the limited test data, only two GSD curves were used in the optimization procedure. For the simplicity, all the selected constant p' tests were marked as "D-1, 2, 3, 4, 5, 6, and 7". Table 8 shows the initial void ratio and confining pressure for each selected test. Based on the necessary number of tests suggested previously, the tests of D-1, 2, 3, 4 and 5 were used as the objectives in the optimization, and the tests of D-6 and 7 were used for validation.

Following the proposed procedure, the parameters of the adopted breakage model for Dog's bay sand were identified by using NMGA. Table 9 summarizes the optimal parameters. Using the optimal parameters, the objective tests were first simulated. Fig. 8 (a-d) shows the comparison of isotropic compression test, constant p' tests and GSD curves between the optimal simulations and experiments. Then, three additional drained constant p' triaxial tests were used for validation, as shown in Fig. 8 (e-f). It can be seen that the simulations generally well agree with the measurements, which demonstrates that the identified parameters of the adopted breakage model by the proposed procedure are reliable.

5.2. Modelling of pile driving tests

5.2.1 Description of pile driving tests

A series of centrifuge pile penetration tests on Dog's bay sand under an acceleration of 100 g performed by Klotz and Coop (2001) were simulated by using the adopted breakage model with the optimal parameters. The pile is closed-ended and the diameter is 16 mm. The maximum penetration into the sand is about 375 mm, which equals to 1.6 m in diameter and 37.5 m in height for the real case. The cylindrical container has an internal diameter of D = 40 cm and a height of 63 cm with rigid walls to avoid lateral displacements of soil, which equals to 32 m and 54 m for the real case,

respectively. Two different initial void ratios (e_0 = 1.53 and e_0 = 1.39) of Dog's bay sand were used in the centrifuge test. The pile was pushed into the sand at a speed of 0.02 m/s for both tests in real case (Klotz and Coop, 2001).

5.2.2 Model implementation into finite element code

The Coupled Eulerian Lagrangian (CEL) method in the ABAQUS (Hibbitt et al., 2001) that captures the advantages of both the Lagrangian and the Eulerian method, which is effective on solving the large deformation problems. In numerical analyses using this CEL method the Eulerian material is tracked as it flows through the mesh by computing its Eulerian volume fraction (EVF). Each Eulerian element is designated by a percentage, which represents the portion of that element filled with a Eulerian material. For simulating pile penetration tests, the Coupled Eulerian Lagrangian (CEL) method in ABAQUS was adopted to deal with the analysis of large deformation at the edge of pile penetration (Hamann et al., 2015; Qiu et al., 2011). The adopted breakage model was implemented into ABAQUS as a user defined material model via VUMAT (user defined material model for ABAQUS/Explicit) to simulate Dog's bay sand. The explicit time integration scheme was used in the implementation in Abaqus/Explicit (Hibbitt et al., 2001). The central difference rule is employed for the solution of the non-linear system of differential equations. The unknown solution for the next time step can be found directly from the solution of the previous time step, such that no iteration is needed.

The model implementation was examined by simulating above triaxial tests on limestone grains and carbonate sand. All simulation results were the same as those obtained by the single integration point program, which validated the model implementation.

5.2.3 Finite element model

Due to the axial symmetry of the problem, a three-dimensional finite element (FE) model for 1 quarter of the model test was established as illustrated in Fig. 9. The dimension of FE model was same as the equivalent real case of model tests. The bottom of FE model was fixed in three directions. The lateral of FE model was fixed in horizontal directions and the vertical direction was free. The pile was modeled as a rigid body. The Dog's bay sand was modeled by using 62000 Eulerian elements. The upper 2 meters were modeled by void to allow the Eulerian material to flow into

during the pile penetration. The contact between the pile and Dog's bay sand was described by the classical Coulomb friction law with a friction coefficient $\mu = \tan(\phi_\mu/2) = 0.40$. According to Klotz and Coop (2001), the initial stress state before loading was generated by self-weight with $K_0 = 0.305$ according to Jacky's formula. The parameters of Dog's bay sand optimized previously in Table 9 were used for the simulation. The total penetration displacement is 37.5 m and the penetration speed was 0.02 m/s.

5.2.4 Results and comparisons

Fig. 10 shows the comparisons of "q_b - z" curves between the measurements and the simulations for two centrifuge pile penetration tests, where q_b represents the base resistance and z is the penetration displacement of the pile. A general good agreement between the predictions and observations demonstrates that the adopted model has an outstanding ability in capturing the pile penetration behavior accounting for the effect of grain breakage, and the identified model parameters are reliable. Due to the instability and the numerical oscillation of explicit calculations, the obtained curves are not always smooth.

Taking the simulation with e_0= 1.53 as example, the information of void ratio, deviatoric plastic strain, modified breakage index B_r^* and mean effective stress during the process of pile driven is presented. Fig. 11 shows the distribution of these information at a penetration depth of 5 m, 10m and 37 m. It can be seen that the mean effective stress around the pile head is increased with increasing the pile penetration depth. The increased mean effective stress and deviatoric plastic strain result in globally decreasing the void ratio so that make the sand denser, and simultaneously causes more breakage of sand grains due to increasing plastic work. The maximum value of void ratio reached to 1.639 due to the dilatancy effect during the pile penetration, especially in the area close to the top surface in sand surrounding the pile. Fig. 12 presents the distribution of breakage index with different profiles in surrounding soil at the distance of 0, 0.2, 0.4, and 0.8 m from pile at the penetration depth of 37 m. Fig. 13 shows the distributions of breakage index along the radius (distance from the pile) at penetration depths of 5 m, 10m, and 37 m. It seems that the crushing-influenced zone predicted by the breakage model is within approximately a radius of pile

from the shaft. However, it is a pity that the breakage growth cannot be compared against the experimental data since it is not available.

6. Conclusions

An efficient optimization procedure to identify the breakage model's parameters for easily crushable sand has been proposed using which the capacity of offshore pile driving was numerically estimated.

In the optimization procedure, a newly developed elasto-plastic constitutive model accounting for grain breakage was adopted to simulate the objective tests for measuring the error between the simulations and objective tests. To improve the performance of identification, a new optimization algorithm NMGA was proposed by implementing the Nelder-Mead Simplex into a recently developed real coded genetic algorithm. First, the computational effectiveness and efficiency of the proposed NMGA were evaluated by comparing with the RCGA and the MOGA-II algorithms. All the three optimization methods were applied to conduct the same parameter identification. In the optimization, the objective was three synthetic drained triaxial tests generated by the adopted breakage model with a set of parameters representing an easily crushable sand. The results show that the performance of proposed NMGA on search ability and convergence speed is better than the RCGA and MOGA-II.

Then, the proposed optimization procedure was examined by identifying the model parameters of limestone grains adopting all the experimental tests as the objective. The results show that the obtained optimal parameters are accurate and reasonable. To reduce the cost of parameters determination, the minimum number of tests involved in the objective was investigated. The results indicate that five tests including one test at low confining pressure and one test at high confining pressure are sufficient for the parameter identification, which can be adopted in testing code for practice.

Finally, the adopted breakage model's parameters of a typically carbonate sand (Dog's bay sand) were optimized using the proposed procedure. The Coupled Eulerian Lagrangian based large deformation finite element analysis combined with the breakage model was carried out for pile driving in the same sand for which the finite element implementation of the model was also

conducted. Good agreement was achieved between the simulations and measurements. Furthermore, the role of grain breakage in bearing capacity of driven pile was numerically discussed.

Overall, it can be concluded that the proposed optimization procedure is efficient and reliable on identifying the model parameters for easily crushable sand, and the developed numerical platform is applicable for estimating the capacity of pile driving in this kind of sand.

Acknowledgments

The financial support for this research came from the National Natural Science Foundation of China (Grant nos. 51579179), the Region Pays de la Loire of France (project RI-ADAPTCLIM) and the Macau Science and Technology Development Fund FDCT/125/2014/A3.

Appendix I - *Nelder-Mead algorithm*

Initialization. Evaluate the function value at each vertex point and order the n+1 vertices to satisfy $f(X_1) \leq f(X_2) \leq \ldots \leq f(X_{n+1})$.

Reflection. Compute the reflection point X_r as follows,

$$X_r = \bar{X} + \alpha \cdot \left(\bar{X} - X_{n+1} \right) \quad \text{(A1)}$$

and evaluate $f(X_r)$. If $f(X_1) \leq f(X_r) \leq f(X_n)$, replace X_{n+1} with X_r .

Expansion. If $f(X_r) \leq f(X_1)$ then compute the expansion point X_e from

$$X_e = \bar{X} + \beta \cdot \left(X_r - \bar{X} \right) \quad \text{(A2)}$$

and evaluate $f(X_e)$. If $f(X_r) \leq f(X_e)$, replace X_{n+1} with X_e; otherwise replace X_{n+1} with X_r

Outside Contraction. If $f(X_n) \leq f(X_r) \leq f(X_{n+1})$, compute the outside contraction point

$$X_{oc} = \bar{X} + \gamma \cdot \left(X_r - \bar{X} \right) \quad \text{(A3)}$$

and evaluate $f(X_{oc})$. If $f(X_{oc}) \leq f(X_r)$, replace X_{n+1} with X_{oc}; otherwise go to Shrink.

Inside Contraction. If $f(X_r) \geq f(X_{n+1})$, compute the inside contraction point X_{ic} from

$$X_{ic} = \bar{X} + \gamma \cdot \left(X_r - \bar{X} \right) \quad \text{(A4)}$$

and evaluate $f(X_{ic})$. If $f(X_{ic}) < f(X_{n+1})$, replace X_{n+1} with X_{ic}; otherwise, go to Shrink.

Shrink. For $2 \leq i \leq n+1$, define

$$X_i = X_1 + \delta \left(X_i - X_1 \right) \quad \text{(A5)}$$

where α=1, β=1+2/n, γ=0.75-1/2n and δ=1-1/n; n is number of variables.

References

Cecconi, M., Desimone, A., Tamagnini, C., Viggiani, G.M.B., 2002. A constitutive model for granular materials with grain crushing and its application to a pyroclastic soil. International Journal for Numerical and Analytical Methods in Geomechanics 26 (15), 1531-1560.

Chelouah, R., Siarry, P., 2003. Genetic and Nelder–Mead algorithms hybridized for a more accurate global optimization of continuous multiminima functions. European Journal of Operational Research 148 (2), 335-348.

Chen, Q., Indraratna, B., Carter, J.P., Nimbalkar, S., 2015. Isotropic–kinematic hardening model for coarse granular soils capturing particle breakage and cyclic loading under triaxial stress space. Canadian Geotechnical Journal 53 (4), 646-658.

Coop, M., 1990. The mechanics of uncemented carbonate sands. Géotechnique 40 (4), 607-626.

Coop, M., Sorensen, K., Freitas, T.B., Georgoutsos, G., 2004. Particle breakage during shearing of a carbonate sand. Géotechnique 54 (3), 157-163.

Daouadji, A., Hicher, P.-Y., Rahma, A., 2001. An elastoplastic model for granular materials taking into account grain breakage. European Journal of Mechanics-A/Solids 20 (1), 113-137.

Durand, N., Alliot, J.-M., 1999. A combined nelder-mead simplex and genetic algorithm, Proceedings of the Genetic and Evolutionary Computation Conference GECCO, pp. 1-7.

Einav, I., 2007. Breakage mechanics—part I: theory. Journal of the Mechanics and Physics of Solids 55 (6), 1274-1297.

Gao, F., Han, L., 2012. Implementing the Nelder-Mead simplex algorithm with adaptive parameters. Computational Optimization and Applications 51 (1), 259-277.

Guyon E., Troadec J.-P., 1994. Du sac de billes au tas de sable, Editions Odile JACOB Sciences.

Hamann, T., Qiu, G., Grabe, J., 2015. Application of a Coupled Eulerian–Lagrangian approach on pile installation problems under partially drained conditions. Computers and Geotechnics 63, 279-290.

Hibbitt, Karlsson, Sorensen, 2001. ABAQUS/Explicit: User's Manual. Hibbitt, Karlsson and Sorenson.

Hu, W., Yin, Z.Y., Dano, C., Hicher, P.Y., 2011. A constitutive model for granular materials considering grain breakage. Science China-Technological Sciences 54 (8), 2188-2196.

Jin, Y.-F., Wu, Z.-X., Yin, Z.-Y., Shen, J.S., 2017a. Estimation of critical state-related formula in advanced constitutive modeling of granular material. Acta Geotechnica. doi: 10.1007/s11440-017-0586-5

Jin, Y.-F., Yin, Z.-Y., Riou, Y., Hicher, P.-Y., 2017b. Identifying creep and destructuration related soil parameters by optimization methods. KSCE Journal of Civil Engineering 21 (4), 1123-1134.

Jin, Y.-F., Yin, Z.-Y., Shen, S.-L., Hicher, P.-Y., 2016a. Investigation into MOGA for identifying parameters of a critical-state-based sand model and parameters correlation by factor analysis. Acta Geotechnica 11 (5), 1131-1145.

Jin, Y.-F., Yin, Z.-Y., Shen, S.-L., Hicher, P.-Y., 2016b. Selection of sand models and identification of parameters using an enhanced genetic algorithm. International Journal for Numerical and Analytical Methods in Geomechanics 40 (8), 1219-1240.

Jin, Y.-F., Yin, Z.-Y., Shen, S.-L., Zhang, D.-M., 2017c. A new hybrid real-coded genetic algorithm and its application to parameters identification of soils. Inverse Problems in Science and Engineering 25 (9), 1343-1366.

Jin, Y.-F., Yin, Z.-Y., Shen, S.L., Hicher, P.Y., 2016c. Selection of sand models and identification of parameters using an enhanced genetic algorithm. International Journal for Numerical and Analytical Methods in Geomechanics 40, 1219-1240.

Klotz, E., Coop, M., 2001. An investigation of the effect of soil state on the capacity of driven piles in sands. Géotechnique 51 (9), 733-751.

Kong, Y., Xu, M., Song, E., 2017. An elastic-viscoplastic double-yield-surface model for coarse-grained soils considering particle breakage. Computers and Geotechnics 85, 59-70.

Levasseur, S., Malécot, Y., Boulon, M., Flavigny, E., 2008. Soil parameter identification using a genetic algorithm. International Journal for Numerical and Analytical Methods in Geomechanics 32 (2), 189-213.

Liu, M., Gao, Y., 2016. Constitutive Modeling of Coarse-Grained Materials Incorporating the Effect of Particle Breakage on Critical State Behavior in a Framework of Generalized Plasticity. International Journal of Geomechanics 0 (0), 04016113.

Liu, Y.-J., Li, G., Yin, Z.-Y., Dano, C., Hicher, P.-Y., Xia, X.-H., Wang, J.-H., 2014. Influence of grading on the undrained behavior of granular materials. Comptes Rendus Mecanique 342 (2), 85-95.

Lo, K.Y., RoY, M., 1973. Response of particulate materials at high pressures. Soils and Foundations 13 (1), 61-76.Miao, G., Airey, D., 2013. Breakage and ultimate states for a carbonate sand. Géotechnique 63 (14), 1221-1229.

Pal, S., Wije Wathugala, G., Kundu, S., 1996. Calibration of a constitutive model using genetic algorithms. Computers and Geotechnics 19 (4), 325-348.

Papon, A., Riou, Y., Dano, C., Hicher, P.Y., 2012. Single-and multi-objective genetic algorithm optimization for identifying soil parameters. International Journal for Numerical and Analytical Methods in Geomechanics 36 (5), 597-618.

Qiu, G., Henke, S., Grabe, J., 2011. Application of a Coupled Eulerian–Lagrangian approach on geomechanical problems involving large deformations. Computers and Geotechnics 38 (1), 30-39.

Randolph, M., Cassidy, M., Gourvenec, S., Erbrich, C., 2005. Challenges of offshore geotechnical engineering, Proceedings of the international conference on soil mechanics and geotechnical engineering. AA BALKEMA PUBLISHERS, p. 123.

Randolph, M., Dolwin, J., Beck, R., 1994. Design of driven piles in sand. Géotechnique 44 (3), 427-448.

Richart, F., Hall, J., Woods, R., 1970. Vibrations of soils and foundations. International Series in Theoretical and Applied Mechanics. Englewood Cliffs, NJ: Prentice-Hall.

Rokonuzzaman, M., Sakai, T., 2010. Calibration of the parameters for a hardening–softening constitutive model using genetic algorithms. Computers and Geotechnics 37 (4), 573-579.

Russell, A.R., Khalili, N., 2004. A bounding surface plasticity model for sands exhibiting particle crushing. Canadian Geotechnical Journal 41 (6), 1179-1192.

Samarajiva, P., Macari, E.J., Wathugala, W., 2005. Genetic algorithms for the calibration of constitutive models for soils. International Journal of Geomechanics 5 (3), 206-217.

Sobol, I.M., 1967. On the distribution of points in a cube and the approximate evaluation of integrals. Zhurnal Vychislitel'noi Matematiki i Matematicheskoi Fiziki 7 (4), 784-802.

Xiao, Y., Liu, H., 2016. Elastoplastic Constitutive Model for Rockfill Materials Considering Particle Breakage. International Journal of Geomechanics 0 (0), 04016041.

Yao, Y.-P., Yamamoto, H., Wang, N.-D., 2008a. Constitutive model considering sand crushing. Soils and Foundations 48 (4), 603-608.

Yao, Y., Hou, W., Zhou, A., 2009. UH model: three-dimensional unified hardening model for overconsolidated clays. Géotechnique 59 (5), 451-469.

Yao, Y., Lu, D., Zhou, A., Zou, B., 2004a. Generalized non-linear strength theory and transformed stress space. Science in China Series E: Technological Sciences 47 (6), 691-709.

Yao, Y., Sun, D., Luo, T., 2004b. A critical state model for sands dependent on stress and density. International Journal for Numerical and Analytical Methods in Geomechanics 28 (4), 323-337.

Yao, Y., Sun, D., Matsuoka, H., 2008b. A unified constitutive model for both clay and sand with hardening parameter independent on stress path. Computers and Geotechnics 35 (2), 210-222.

Ye, L., Jin, Y.-F., Shen, S.-L., Sun, P.-P., Zhou, C., 2016. An efficient parameter identification procedure for soft sensitive clays. Journal of Zhejiang University SCIENCE A 17 (1), 76-88.

Yin, Z.-Y., Hicher, P.-Y., Dano, C., Jin, Y.-F., 2016. Modeling Mechanical Behavior of Very Coarse Granular Materials. Journal of engineering mechanics, C4016006.

Yin, Z.-Y., Jin, Y.-F., Shen, J.S., Hicher, P.-Y., 2017a. Optimization techniques for identifying soil parameters in geotechnical engineering: Comparative study and enhancement. International Journal for Numerical and Analytical Methods in Geomechanics, n/a-n/a.

Yin, Z.-Y., Jin, Y.-F., Shen, S.-L., Huang, H.-W., 2017b. An efficient optimization method for identifying parameters of soft structured clay by an enhanced genetic algorithm and elastic–viscoplastic model. Acta Geotechnica 12 (4), 849-867.

Zhang, C., Nguyen, G., Einav, I., 2013. The end-bearing capacity of piles penetrating into crushable soils. Géotechnique 63 (5), 341-354.

Zhang, C., Yang, Z., Nguyen, G., Jardine, R., Einav, I., 2014. Theoretical breakage mechanics and experimental assessment of stresses surrounding piles penetrating into dense silica sand. Géotechnique Letters 4 (January-March), 11-16.

Zhang, Y.D., Buscarnera, G., 2017. A rate-dependent breakage model based on the kinetics of crack growth at the grain scale. Géotechnique, 1-15.

Zhang, Y.D., Buscarnera, G., Einav, I., 2016. Grain size dependence of yielding in granular soils interpreted using fracture mechanics, breakage mechanics and Weibull statistics. Géotechnique 66 (2), 1-12.

Tables

Table 1 Search domain and intervals of parameters for adopted grain breakage model

Groups	Elastic		Critical-sate			Plastic		Gain breakage		
Parameters	K_0	n	e_{ref}	λ	ϕ_u	G_p	A_d	p_{m0}	a	b
Lower bound	10	0.2	0.5	0.01	20	1	0	50	50	0
Upper bound	400	0.8	2.0	0.5	50	50	5.0	10000	10000	20
Step size	10	0.01	0.001	0.001	1	0.1	0.1	10	10	1

Table 2 Optimal parameters obtained by NMGA, RCGA and MOGA-II from synthetic data

Parameters	K_0	n	e_{ref}	λ	ϕ	G_p	A_d	p_{m0}	a	b	Objective error / %
Preset	70	0.66	1.000	0.05	35	5.0	1.0	500	150	10	-
NMGA	70	0.66	1.000	0.05	35	5.0	1.0	500	150	10	0.00
RCGA	65	0.47	0.996	0.086	35	12.9	0.9	560	150	4	2.70
MOGA-II	60	0.53	1.019	0.065	34	10.2	0.8	620	150	8	2.22

Table 3 A series of triaxial tests on Limestone grains with initial void ratio (e_0 = 0.81)

Test number	①	②	③	④	⑤	⑥	⑦	⑧	⑨
e_0 before shearing	0.8	0.77	0.75	0.726	0.67	0.606	0.510	0.448	0.397
σ'_c / kPa	172	345	517	690	1380	2760	5520	8275	11030

Table 4 Optimal parameters with the optimal errors of testing on Limestone grains

Method	Optimal parameters							Average error (%)
	e_{ref}	λ	ϕ	G_p	A_d	a	b	
NMGA	0.930	0.107	41	32.1	2.1	2300	3	5.83
RCGA	0.890	0.080	41	30	2.7	2350	7	6.82
MOGA-II	0.884	0.066	42	20.2	2.3	2300	10	7.44

Table 5 Optimal parameters and errors for different weights of GSD

No.	weight	Optimal parameters							Objective error (%)	Total average error (%)
	A	e_{ref}	λ	ϕ (°)	G_p	A_d	a	b		
1	1	0.99	0.110	42	21.6	1.6	350	2	7.35	12.96
2	0.7	0.95	0.115	41	31	1.9	1800	2	6.09	6.45
3	0.5	0.95	0.117	41	33.8	1.7	1950	2	5.26	6.49
4	0.3	0.95	0.116	41	33.7	1.8	1950	2	4.46	6.47
5	0	1.42	0.189	34	4.3	1.9	1800	11	0.34	154

Table 6 Optimal parameters and errors of different combination of tests

No.	Combination of tests	Optimal parameters							Objective error (%)	Total average error (%)
		e_{ref}	λ	ϕ (°)	G_p	A_d	a	b		
1	①②⑧	0.97	0.131	41	33.0	1.5	1700	1	7.53	8.74
2	①③⑧	0.97	0.128	41	29.4	1.3	2000	1	7.22	8.07
3	①④⑧	0.96	0.129	41	42.0	1.6	2050	1	7.30	8.78
4	①⑤⑧	0.96	0.129	40	34.5	1.6	2050	1	6.18	7.35
5	①⑥⑧	0.97	0.118	41	25.7	1.4	1900	2	5.71	7.04
6	①⑦⑧	0.96	0.115	41	28.1	1.6	1600	2	6.05	6.93
7	①②③⑧	0.95	0.120	41	40.3	1.9	1900	2	5.37	6.61
8	①②④⑧	0.96	0.132	41	48.5	1.8	2050	1	5.78	7.30
9	①②⑤⑧	0.93	0.109	41	41.8	2.1	2250	3	5.90	6.02
10	①②⑥⑧	0.94	0.108	41	32.6	1.9	2050	3	5.97	6.09
11	①②⑦⑧	0.95	0.123	40	34.5	1.9	1750	1	5.50	7.01
12	①③④⑧	0.97	0.140	41	49.3	2.0	2250	1	7.41	8.30
13	①③⑤⑧	0.94	0.118	40	43.2	2.2	2250	2	6.17	6.17
14	①③⑥⑧	0.94	0.108	41	36.3	1.9	2000	3	6.33	6.27
15	①③⑦⑧	0.95	0.118	41	37.8	1.7	1900	2	5.60	6.47
16	①④⑤⑧	0.94	0.111	41	36.4	2.1	2300	3	6.35	5.96
17	①④⑥⑧	0.94	0.114	40	34.3	2.0	2150	2	6.42	6.15
18	①④⑦⑧	0.95	0.124	40	38.0	1.8	1900	1	5.71	6.83
19	①⑤⑥⑧	0.94	0.114	40	33.3	2.1	2240	2	6.33	6.07
20	①⑤⑦⑧	0.95	0.117	40	28.9	1.7	2000	2	5.61	6.44
21	①⑥⑦⑧	0.97	0.119	41	23.4	1.4	1800	2	5.38	6.75
22	①②③④⑧	0.98	0.143	41	40.8	1.8	2350	1	7.43	6.53
23	①②③⑤⑧	0.95	0.124	41	42.8	1.9	2500	2	5.71	6.49
24	①②③⑥⑧	0.93	0.106	41	33.2	2.0	2250	3	5.80	5.92
25	①②③⑦⑧	0.94	0.115	41	38.3	2.0	1800	2	5.37	6.38
26	①②④⑤⑧	0.94	0.114	41	39.9	2.1	2500	3	5.72	6.07
27	①②④⑥⑧	0.93	0.107	41	38.7	2.1	2300	3	5.93	5.96

28	①②④⑦⑧	0.95	0.117	41	36.1	1.8	1800	2	5.26	6.50
29	①②⑤⑥⑧	0.94	0.107	41	29.7	2.0	2200	3	5.94	5.97
30	①②⑤⑦⑧	0.93	0.107	41	33.5	2.0	2100	3	5.68	5.93
31	①②⑥⑦⑧	0.94	0.112	40	29.4	2.0	1900	2	5.09	6.27
32	①③④⑤⑧	0.93	0.110	41	43.4	2.4	2400	3	6.48	5.95
33	①③④⑥⑧	0.93	0.106	41	36.5	2.3	2350	3	6.78	5.93
34	①③④⑦⑧	0.96	0.121	41	32.5	1.7	2100	2	6.25	6.40
35	①③⑤⑥⑧	0.93	0.114	40	42.1	2.2	2400	2	6.48	5.98
36	①③⑤⑦⑧	0.94	0.115	40	35.2	2.2	2150	2	5.96	6.07
37	①③⑥⑦⑧	0.95	0.108	41	25.8	2.0	2050	3	5.58	6.10
38	①④⑤⑥⑧	0.93	0.106	40	34.1	2.5	2300	3	6.34	6.00
39	①④⑤⑦⑧	0.94	0.115	40	34.8	2.1	2200	2	6.06	6.06
40	①④⑥⑦⑧	0.94	0.114	40	34.7	1.9	1900	2	5.55	6.34
41	①⑤⑥⑦⑧	0.94	0.113	40	33.7	2.1	2000	2	5.63	6.21

Table 7 Average optimal parameters and errors for each group of different number of tests

Groups	e_{ref}	λ	ϕ	G_p	A_d	a	b	Range of objective error /%	Total average error /%
3 tests	0.965	0.125	40.8	32.1	1.50	1900	1.3	5.71~7.53	7.80
4 tests	0.948	0.118	40.6	37.2	1.90	2050	2.0	5.37~7.41	6.60
5 tests	0.941	0.114	40.7	35.8	2.05	2200	2.4	5.26~7.43	6.10
8 tests	0.940	0.107	41.0	32.1	2.10	2300	3.0	5.80	5.90

Table 8 A series of triaxial tests on Dog's bay sand (constant mean effective stress)

Tests	D-1	D-2	D-3	D-4	D-5	D-6	D-7
e_0	1.365	1.582	1.557	1.751	1.757	1.744	1.705
σ'_c / kPa	500	500	1000	4000	500	1000	4000

Table 9 Optimal parameters of adopted breakage model with objective error for Dog's bay sand

Parameters	K_0	n	e_{ref}	λ	ϕ /°	G_p	A_d	p_{m0} /kPa	a	b	Error (%)
Value	160	0.56	1.79	0.0148	44	19	0.5	670	2500	10	6.62

Figure captions

Figure 1

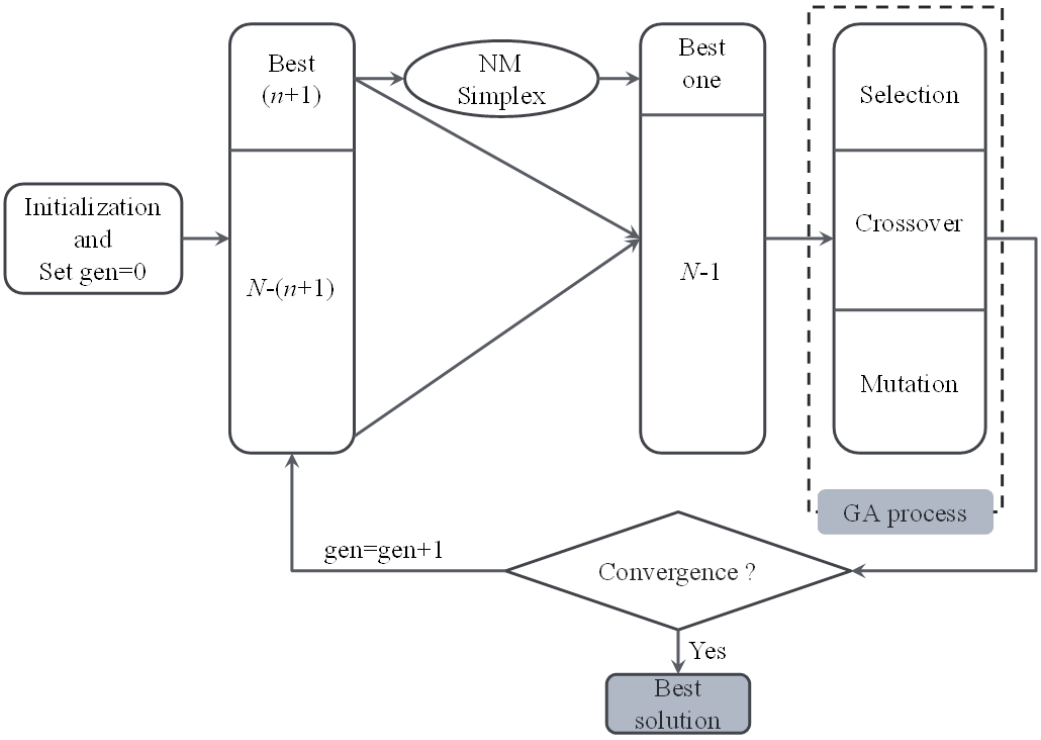
Initialization and Set gen=0
Best (n+1)
N-(n+1)
NM Simplex
Best one
N-1
Selection
Crossover
Mutation
GA process
gen=gen+1
Convergence ?
Yes
Best solution

Figure 2

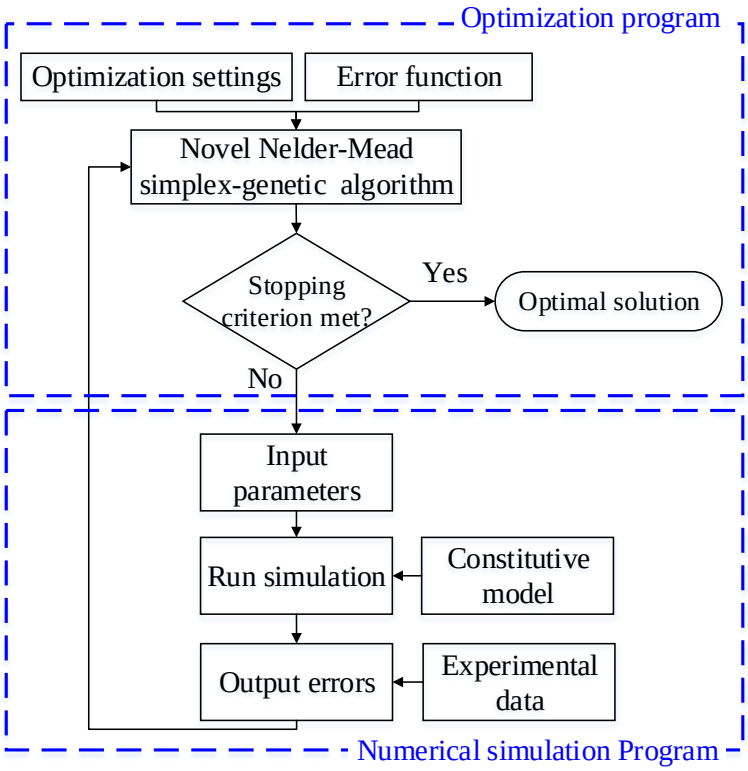
Optimization program
Optimization settings
Error function
Novel Nelder-Mead simplex-genetic algorithm
Stopping criterion met?
Yes
Optimal solution
No
Input parameters
Run simulation
Constitutive model
Output errors
Experimental data
Numerical simulation Program

Figure 3

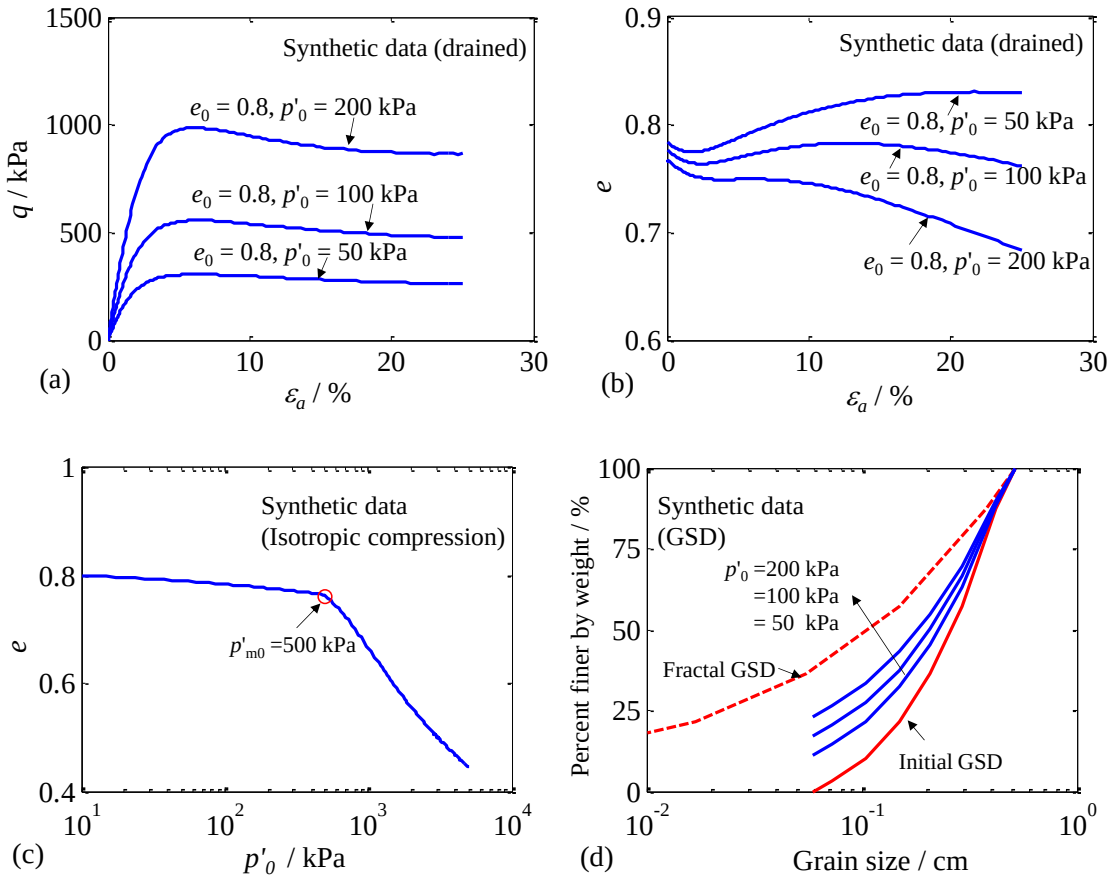
Synthetic data (drained)
e_0 = 0.8, p'_0 = 200 kPa
e_0 = 0.8, p'_0 = 100 kPa
e_0 = 0.8, p'_0 = 50 kPa
q / kPa
ε_a / %
(a)
Synthetic data (drained)
e_0 = 0.8, p'_0 = 50 kPa
e_0 = 0.8, p'_0 = 100 kPa
e_0 = 0.8, p'_0 = 200 kPa
e
ε_a / %
(b)
Synthetic data
(Isotropic compression)
p'_{m0} =500 kPa
e
p'_0 / kPa
(c)
Synthetic data
(GSD)
p'_0 =200 kPa
=100 kPa
= 50 kPa
Fractal GSD
Initial GSD
Percent finer by weight / %
Grain size / cm
(d)

Figure 4

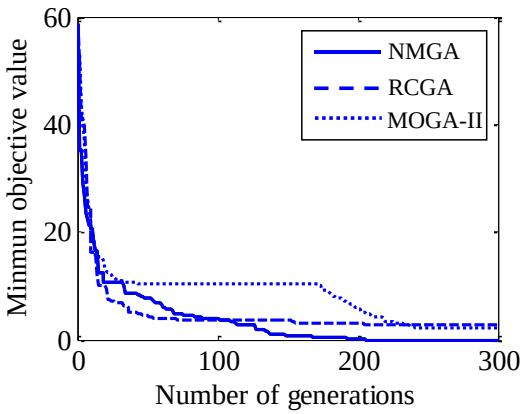
60
40
20
0
0
100
200
300
Minmun objective value
Number of generations
NMGA
RCGA
MOGA-II

Figure 5

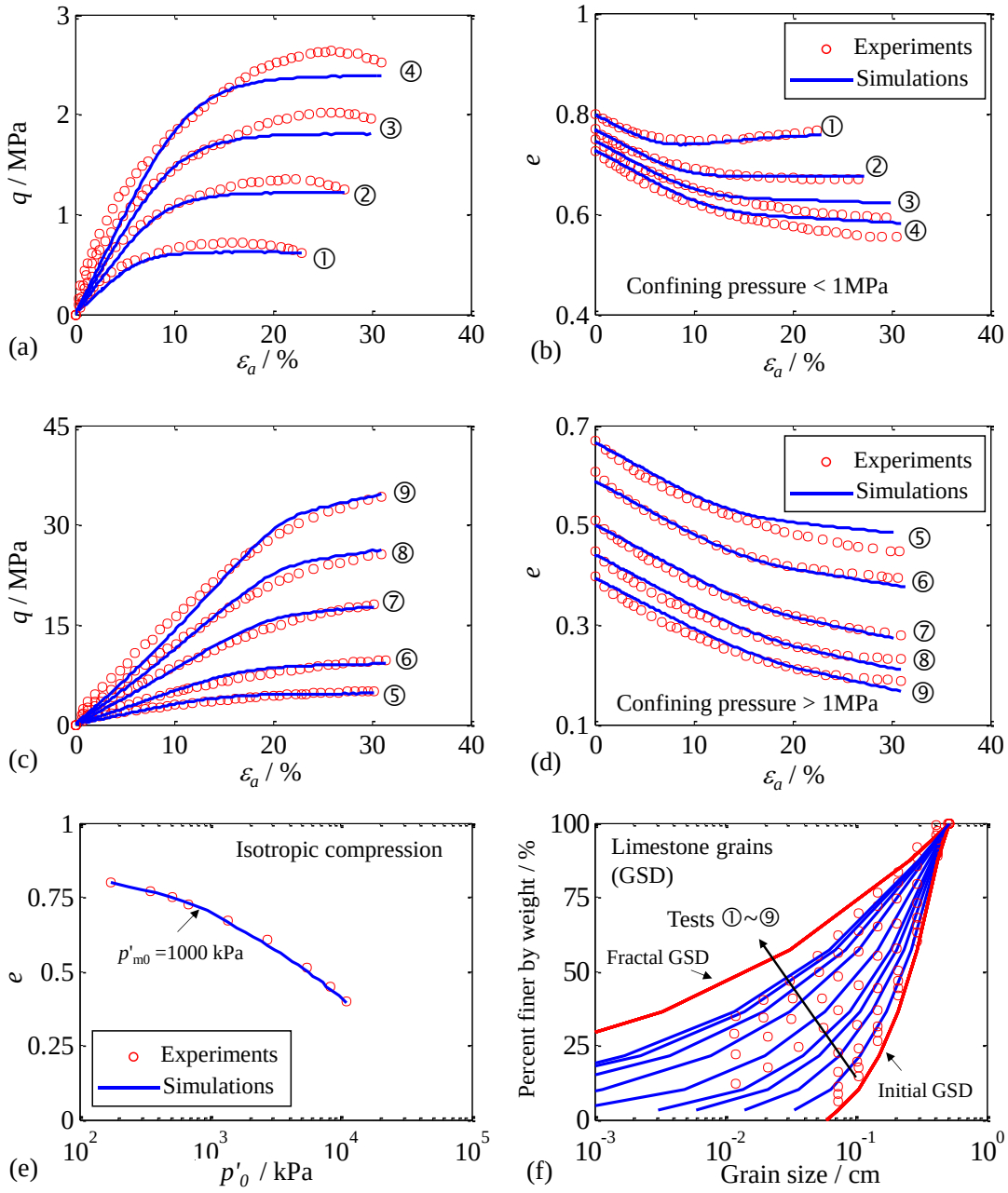
q / MPa
ε_a / %
(a)
①
②
③
④
e
Experiments
Simulations
Confining pressure < 1MPa
(b)
⑤
⑥
⑦
⑧
⑨
Confining pressure > 1MPa
(c)
(d)
Isotropic compression
p'_{m0} =1000 kPa
p'_0 / kPa
(e)
Limestone grains
(GSD)
Tests ①~⑨
Fractal GSD
Initial GSD
Percent finer by weight / %
Grain size / cm
(f)

Figure 6

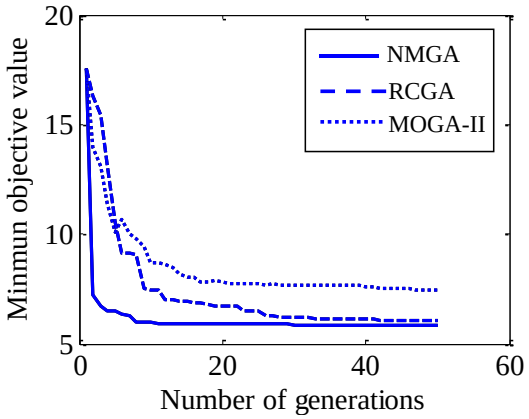
20
15
10
5
0
20
40
60
Minmun objective value
Number of generations
NMGA
RCGA
MOGA-II

Figure 7

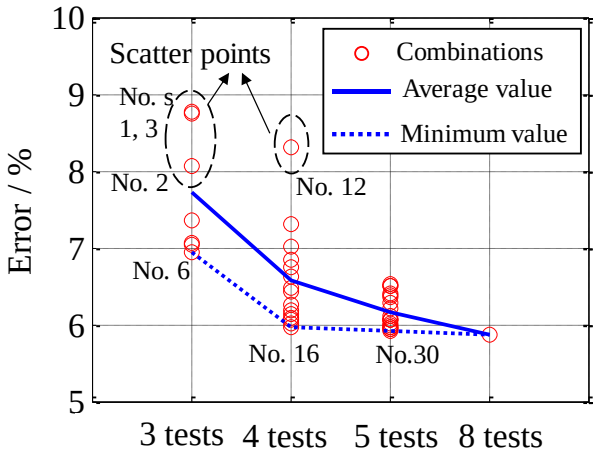
Scatter points
Combinations
Average value
Minimum value
No. s
1, 3
No. 2
No. 12
No. 6
No. 16
No.30
Error / %
10
9
8
7
6
5
3 tests
4 tests
5 tests
8 tests

Figure 8

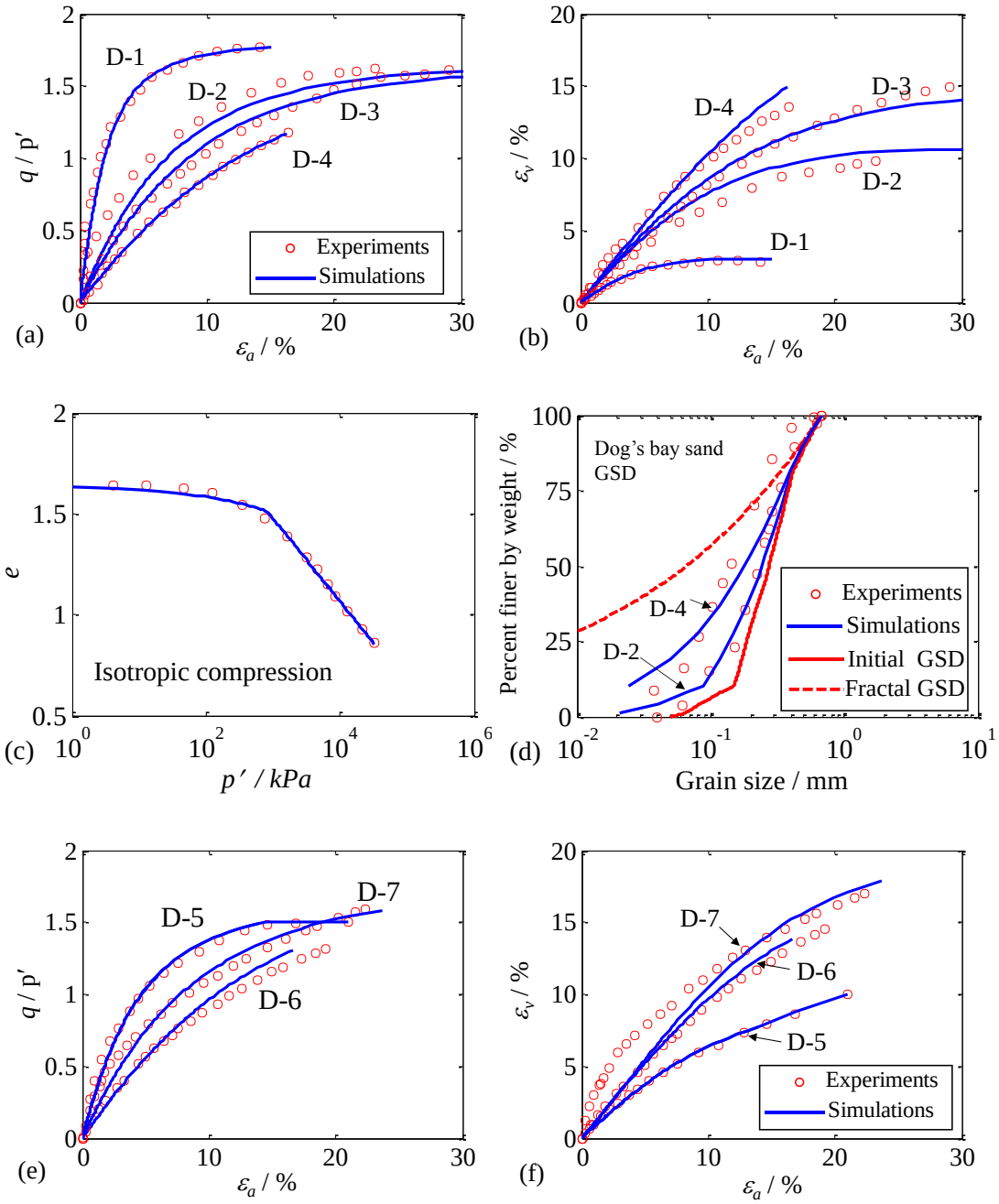
D-1
D-2
D-3
D-4
Experiments
Simulations
q / p′
ε_a / %
(a)
ε_v / %
(b)
e
Isotropic compression
p′ / kPa
(c)
Dog's bay sand GSD
Percent finer by weight / %
Initial GSD
Fractal GSD
Grain size / mm
(d)
D-5
D-6
D-7
(e)
(f)

Figure 9

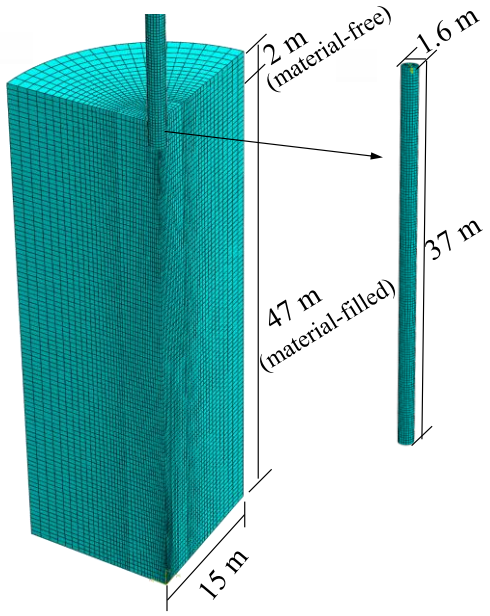

Figure 10

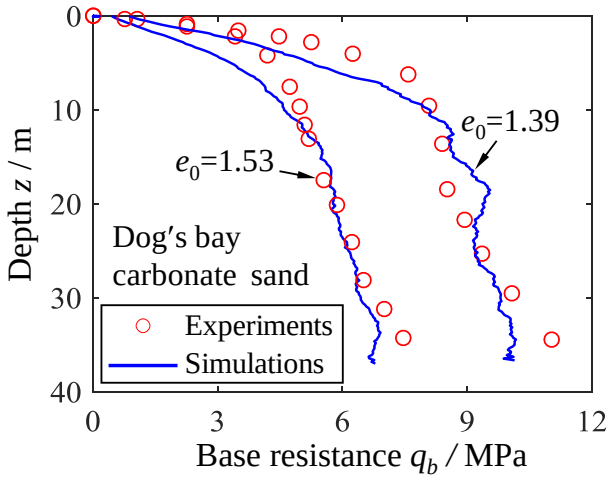
0
10
20
30
40
Depth z / m
0
3
6
9
12
Base resistance q_b / MPa
e_0=1.39
e_0=1.53
Dog's bay
carbonate sand
Experiments
Simulations

Figure 11

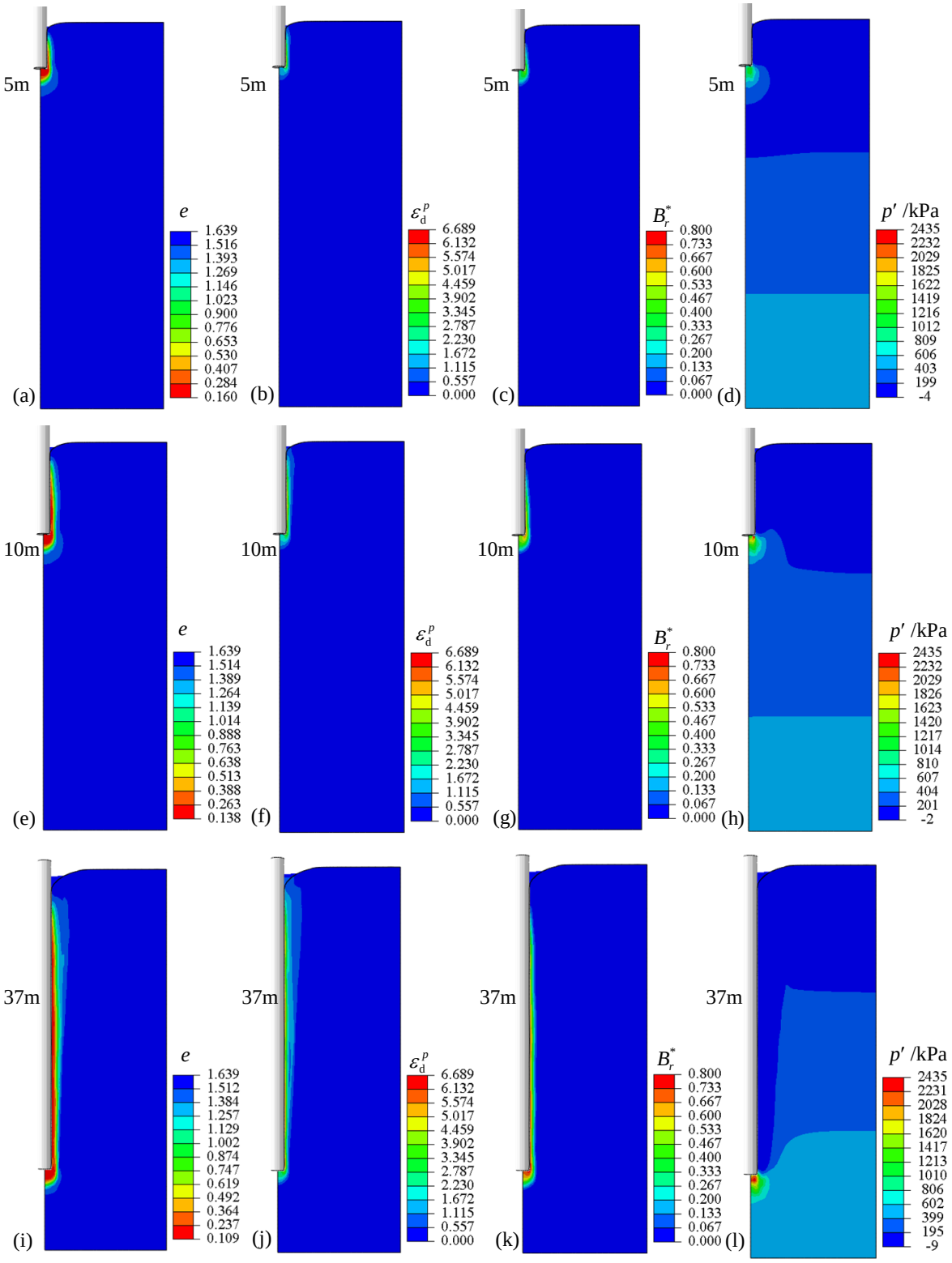
5m
e
1.639
1.516
1.393
1.269
1.146
1.023
0.900
0.776
0.653
0.530
0.407
0.284
0.160
(a)
5m
ε_d^p
6.689
6.132
5.574
5.017
4.459
3.902
3.345
2.787
2.230
1.672
1.115
0.557
0.000
(b)
5m
B_r^*
0.800
0.733
0.667
0.600
0.533
0.467
0.400
0.333
0.267
0.200
0.133
0.067
0.000
(c)
5m
p′ /kPa
2435
2232
2029
1825
1622
1419
1216
1012
809
606
403
199
-4
(d)
10m
e
1.639
1.514
1.389
1.264
1.139
1.014
0.888
0.763
0.638
0.513
0.388
0.263
0.138
(e)
10m
ε_d^p
6.689
6.132
5.574
5.017
4.459
3.902
3.345
2.787
2.230
1.672
1.115
0.557
0.000
(f)
10m
B_r^*
0.800
0.733
0.667
0.600
0.533
0.467
0.400
0.333
0.267
0.200
0.133
0.067
0.000
(g)
10m
p′ /kPa
2435
2232
2029
1826
1623
1420
1217
1014
810
607
404
201
-2
(h)
37m
e
1.639
1.512
1.384
1.257
1.129
1.002
0.874
0.747
0.619
0.492
0.364
0.237
0.109
(i)
37m
ε_d^p
6.689
6.132
5.574
5.017
4.459
3.902
3.345
2.787
2.230
1.672
1.115
0.557
0.000
(j)
37m
B_r^*
0.800
0.733
0.667
0.600
0.533
0.467
0.400
0.333
0.267
0.200
0.133
0.067
0.000
(k)
37m
p′ /kPa
2435
2231
2028
1824
1620
1417
1213
1010
806
602
399
195
-9
(l)

Figure 12

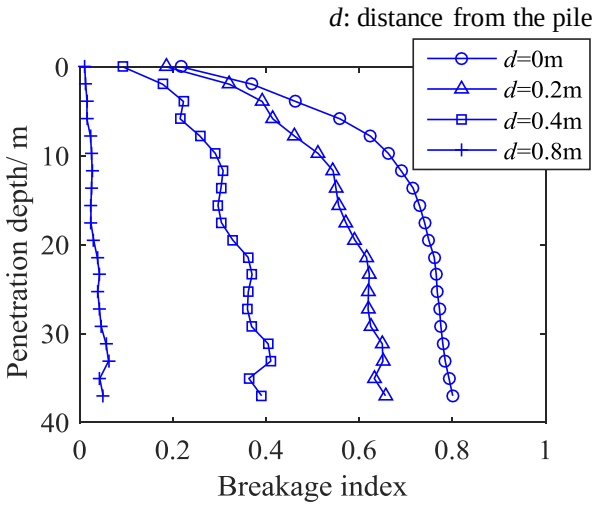
d: distance from the pile
d=0m
d=0.2m
d=0.4m
d=0.8m
Penetration depth/ m
0
10
20
30
40
0
0.2
0.4
0.6
0.8
1
Breakage index

Figure 13

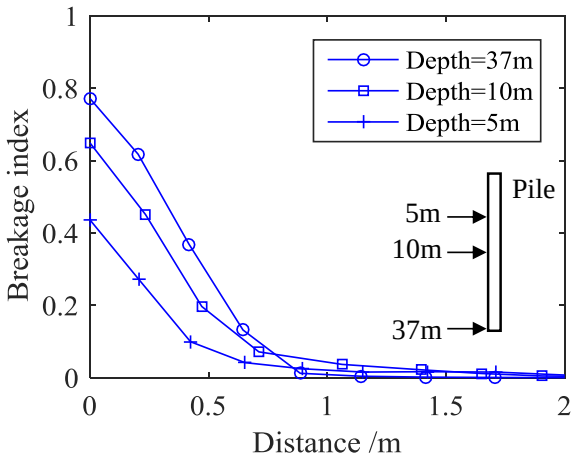
Depth=37m
Depth=10m
Depth=5m
Pile
5m
10m
37m
Breakage index
Distance /m
0
0.2
0.4
0.6
0.8
1
0
0.5
1
1.5
2